



HAL
open science

Superparamagnetic iron oxide nanoparticles (SPIONs)-loaded Trojan microparticles for targeted aerosol delivery to the lung

Frederic Tewes, Carsten Ehrhardt, Anne Marie Healy

► **To cite this version:**

Frederic Tewes, Carsten Ehrhardt, Anne Marie Healy. Superparamagnetic iron oxide nanoparticles (SPIONs)-loaded Trojan microparticles for targeted aerosol delivery to the lung. *European Journal of Pharmaceutics and Biopharmaceutics*, 2014, 86, pp.98 - 104. 10.1016/j.ejpb.2013.09.004 . inserm-01102561

HAL Id: inserm-01102561

<https://inserm.hal.science/inserm-01102561>

Submitted on 13 Jan 2015

HAL is a multi-disciplinary open access archive for the deposit and dissemination of scientific research documents, whether they are published or not. The documents may come from teaching and research institutions in France or abroad, or from public or private research centers.

L'archive ouverte pluridisciplinaire **HAL**, est destinée au dépôt et à la diffusion de documents scientifiques de niveau recherche, publiés ou non, émanant des établissements d'enseignement et de recherche français ou étrangers, des laboratoires publics ou privés.

1 **Superparamagnetic iron oxide nanoparticles (SPIONs)-loaded**
2 **Trojan microparticles for targeted aerosol delivery to the lung**

3 Frederic Tewes^{1,2}, Carsten Ehrhardt¹ and Anne Marie Healy^{1*}

4 1- School of Pharmacy and Pharmaceutical Sciences, Trinity College Dublin, Panoz
5 Institute, College Green, Dublin 2, Ireland.

6

7 2- INSERM U 1070, Pôle Biologie-Santé, Faculté de Médecine & Pharmacie,
8 Université de Poitiers, 40 av. du Recteur Pineau, 86022 Poitiers Cedex, France

9

10 * To whom correspondence should be sent. Ph.: 00 353 1896 1444, e-mail:
11 healyam@tcd.ie

12

13 **Abstract**

14 Targeted aerosol delivery to specific regions of the lung may improve therapeutic
15 efficiency and minimise unwanted side effects. It could potentially be achieved with
16 porous microparticles loaded with superparamagnetic iron oxide nanoparticles (SPIONs)
17 — in combination with a target-directed magnetic gradient field. As a proof of concept of
18 this hypothesis, the aim of this study was to formulate and evaluate the aerodynamic
19 properties of SPIONs-loaded Trojan microparticles after delivery from a dry powder
20 inhaler. Microparticles made of SPIONs, PEG and hydroxypropyl- β -cyclodextrin
21 (HP β CD) were formulated by spray drying and characterised by various physicochemical
22 methods. Aerodynamic properties were evaluated using a next generation cascade
23 impactor (NGI), with or without a magnet positioned at stage 2. Mixing appropriate
24 proportions of SPIONs, PEG and HP β CD allowed Trojan microparticle to be formulated.
25 These particles had a median geometric diameter of $2.8 \pm 0.3 \mu\text{m}$ and were shown to be
26 sensitive to the magnetic field induced by a magnet having a maximum energy product of
27 413.8 kJ/m^3 . However, these particles, characterised by a mass median aerodynamic
28 diameter (MMAD) of $10.2 \pm 2.0 \mu\text{m}$, were considered to be not inhalable. The poor
29 aerodynamic properties resulted from aggregation of the particles. The addition of
30 $(\text{NH}_4)_2\text{CO}_3$ and magnesium stearate (MgST) to the formulation improved the
31 aerodynamic properties of the Trojan particles, and resulted in a MMAD of $2.2 \pm 0.8 \mu\text{m}$.
32 In the presence of a magnetic field on stage 2 of the NGI, the amount of particles
33 deposited at this stage increased 4-fold from $4.8 \pm 0.7\%$ to $19.5 \pm 3.3\%$. These Trojan
34 particles appeared highly sensitive to the magnetic field and their deposition on most of
35 the stages of the NGI was changed in the presence compared to the absence of the

36 magnet. If loaded with a pharmaceutical active ingredient, these particles may be useful
37 for treating localised lung disease such as cancer nodules or bacterial infectious foci.

38

39 **Introduction**

40 Pharmacotherapy of lung diseases often involves direct delivery of active pharmaceutical
41 ingredients (APIs) by pulmonary inhalation. However, despite the progress in aerosol
42 delivery to the lung, administration systems are still unable to effectively deliver the dose
43 to the optimal areas of deposition within the respiratory tract. Optimising the deposition
44 pattern of API within the most suitable part of the airways should increase the efficacy of
45 the treatment and reduce side effects. This should be beneficial for treating localised lung
46 diseases, such as respiratory infection and lung cancer, i.e. by targeting foci of bacterial
47 infection or tumour nodules.

48 Superparamagnetic iron oxide nanoparticles (SPIONs), such as nanoparticles of
49 maghemite ($\gamma\text{-Fe}_2\text{O}_3$) or magnetite (Fe_3O_4) offer attractive magnetic properties. However,
50 SPIONs dispersions are unstable at physiological pH and surface modifications are
51 required to increase their stability in aqueous media. SPION coated dispersions are one of
52 the few FDA approved nanoparticles for use as MRI contrast agents [1]. Lately, SPIONs
53 were also envisaged as sensitive devices for magnetic drug targeting after intravenous
54 nanoparticles administration, in combination with a target-directed magnetic gradient
55 field [2-6].

56 This concept has also been applied in an attempt to target dry nanoparticle aerosols
57 within the lung using magnetically driven deposition [7, 8]. However, it has been
58 demonstrated that, even with optimised magnet design, the resulting magnetic forces
59 would not be sufficient to efficiently guide individual SPIONs in a dry-powder aerosol
60 because of their small magnetic moment [9]. In contrast, when a multitude of SPIONs are
61 assembled in an liquid aerosol droplet as a nanomagnetosol, the magnetic moment of the

62 assembly increased, which resulted in aerosols which were guidable by medically
63 compatible magnetic fields [9]. Also, recently, inert SPIONs added to the nebuliser
64 solution were used to guide the aerosol to the affected region of the lung by means of a
65 strong external magnetic field. Various therapeutic agents have been administrated by
66 this technique [10].

67 However, the small size of nanoparticles can lead to particle–particle aggregation,
68 making their physical handling difficult in liquid and dry powder forms [11]. The
69 delivery of API to the lung may be achieved by using dry powder inhalers (DPIs),
70 metered dose inhalers or nebulisers. In the solid form, as in a DPI, pharmaceutical
71 ingredients are usual more stable than in liquid form. Therefore, with the same concept of
72 increasing the magnetic moment, targeted aerosol delivery to a specific area of the lung
73 could also be achieved with Trojan microparticles loaded with SPIONs. Trojan particles
74 are microparticles composed of nanoparticles and additional components used to
75 maintain the nanoparticles together. Once in the body, the microparticles disaggregate
76 and release the nanoparticles. Trojan particles were previously formulated and reported as
77 being an efficient means of administering nanoparticles to the lung by inhalation [11].
78 These nano-in-microparticle systems should allow for higher aerosolisation and delivery
79 efficiency than nanoparticles and permit the focalization of the drug reservoir in the
80 targeted area.

81 To reach the deep lung alveolar region, particles require a 1-5 μm aerodynamic diameter
82 range. This aerodynamic diameter range corresponds to spherical particles of unit density
83 having a 1 - 5 μm geometric diameter range. Iron oxide density is 4.9 g/cm^3 and 5.2
84 g/cm^3 for maghemite and magnetite, respectively. Therefore, the best way to nebulise

85 microparticles composed of iron oxide is to develop porous hybrid particles with a
86 reduced density. In fact, to optimise the efficacy of dry powder inhalation, porous
87 particles with low apparent density were developed [12]. For instance, tobramycin
88 powder was produced using the emulsion-based PulmoSphere technology, producing
89 highly dispersible porous particles [13]. Excipient-free nanoporous microparticles
90 (NPMs) [14-17] prepared by a spray drying process had improved *in vitro* deposition
91 properties compare to non-porous microparticles. Trojan large porous particle composed
92 of polymeric nanoparticles were also formulated by spray drying and exhibited much
93 better flow and aerosolisation properties than the nanoparticles from which they were
94 prepared [11]. Therefore, the aim of this study was to formulate SPIONs-loaded Trojan
95 porous microparticles for aerosol lung magnetic targeting after administration using a dry
96 powder inhaler.

97

98 **1- Materials and methods**

99

100 **2.1 Materials**

101 Hydroxypropyl- β -cyclodextrin (HP β CD) with an average degree of substitution of 0.65
102 (Encapsin™ HPB) was purchased from Janssen Biotech, Olen, Belgium. Linear PEG
103 10kDa (PEG), alkanes with 99.8% purity (hexane, heptane, octane, nonane, decane and
104 undecane), maghemite (Fe₂O₃) nanoparticles (SPIONs) with a mean diameter of 50 nm,
105 magnesium stearate (MgST) and ammonium carbonate ((NH₄)₂CO₃) were all purchased
106 from Sigma-Aldrich, (Dublin, Ireland).

107 **2.2 Methods**

108 **2.2.1 Spray drying**

109 Various suspensions containing SPIONs were spray dried using a B-290 Mini spray dryer
110 (Büchi, Flawil, Switzerland) set in the closed cycle mode with a 2-fluid nozzle. The
111 liquid phase of the suspensions was composed of butyl acetate/methanol/water mixture
112 with a volume ratio 5:5:1., as used previously [18]. The composition of the suspensions is
113 described in Table 1. The spray dryer was operated as follows: Inlet temperature was
114 65°C; feeding pump was set at 30%; spraying N₂ nozzle flow rate was 15 L/min; N₂
115 flowing at 670 NL/h was used as the drying gas. These conditions resulted in an outlet
116 temperature ranging from 36 to 39°C.

117

118 **Table 1: Concentration (g/L) of materials in the spray dried solutions and formulation code.**

	25P- 75H- 5F	25P- 75H- 30F	50P- 50H- 50F	50P- 50H- 50F- CO ₃	100P- 50F	100P- 50F- CO ₃	100H- 50F	50P- 50H- 50F-ST	50P- 50H- 50F- CO ₃ -ST
Fe ₂ O ₃	5	30	50	50	50	50	50	50	50
PEG	25	25	50	50	100	100	0	50	50
HPβCD	75	75	50	50	0	0	100	50	50
(NH ₄) ₂ CO ₃	0	0	0	25	0	25	0	0	25
MgST	0	0	0	0	0	0	0	6	6

119

120 **2.2.2 Scanning electron microscopy (SEM)**

121 SEM micrographs of samples were taken using a Tescan Mira XMU (Tescan s.r.o.,
 122 Czech Republic) electron microscope. The samples were fixed on aluminium stubs and
 123 coated with a 10 nm-thick gold film. Primary electrons were accelerated under a voltage
 124 of 5 kV. Images were formed from the collection of secondary electrons.

125 **2.2.3 Powder X-ray diffraction (XRD)**

126 XRD measurements were conducted on samples placed in a low background silicon
 127 holder, using a Rigaku Miniflex II desktop X-ray diffractometer (Rigaku, Tokyo, Japan).
 128 The samples were scanned over a range of 5 – 40° 2θ at a step size of 0.05°/s as
 129 previously described [19].

130 **2.2.4 Particle size distribution analysis**

131 The geometric particle size distributions (PSD) were determined by laser diffraction
 132 using a Mastersizer 2000 (Malvern Instruments, Worcestershire, UK) with the Scirocco
 133 2000 dry powder feeder to disperse the particles as described previously [19]. The
 134 dispersive air pressure used was 3 bar and vibration feed rate was set to 50%. Data were
 135 analysed based on the equivalent volume median diameter, D_{50} , and the span of the PSD.
 136 Calculation was performed using Mie theory and refractive index part of 2 and absorption

137 part of 1 as optical particle properties (n=2).

138 **2.2.5 Particle true density**

139 The true density of the materials was measured using an Accupyc 1330 Pycnometer
140 (Micromeritics®) with helium (99.995% purity) to determine the volume of accurately
141 weighed samples. Samples were dried prior to measurement for 24 h in a Gallenkamp
142 vacuum oven operating at 600 mbar and 25°C (n=2).

143 **2.2.6 Surface free energy measurement**

144 Measurements were performed at 0% RH or 40% RH and 30°C, (n = 3) using an inverse
145 gas chromatography (iGC) instrument (SMS Ltd., London, UK). Powders were packed
146 into a silanized glass column (300mm x 3mm), and then pre-treated for 1 h at 30°C and
147 0% RH. Then, 250 µL of the probe vapour-helium mixture was injected into the helium
148 flow. All injections of probe vapours were performed at 0.03% v/v of the saturated probe
149 vapour. A flame ionization detector was used to monitor the probes' elution. In acid-base
150 theory, the total surface free energy of a solid (γ_s^T) has 2 main components: a dispersive
151 contribution (γ_s^d) and specific or acid-base contribution (γ_s^{AB}) which are independent and
152 additive. In order to calculate γ_s^d of the particles, alkane probes with a known dispersive
153 contribution (γ_p^d) and a nil specific contribution (γ_p^{AB}) were used. Methane was used as
154 inert reference. At this low % of saturation (0.03% v/v), iGC was used in infinite dilution
155 conditions and γ_s^d was calculated using the method developed by Schultz *et al.* [20].

156 **2.2.7 Aerodynamic particle diameter analysis**

157 The aerodynamic diameter (AD) distribution of the particles was measured using a Next
158 Generation Impactor (NGI) as previously described [19]. The flow rate was adjusted to
159 get a pressure drop of 4 kPa in the powder inhaler (Handihaler®, Boeringher Ingelheim,
160 Ingelheim, Germany) and the time of aspiration was adjusted to obtain 4 L. The inhaler

161 was filled with gelatin n°3 capsule loaded with 20 ± 2 mg of powder ($n = 3$). After inhaler
162 actuation, particle deposition on the NGI was determined by the SPIONs assay as
163 described below. The amount of particles recovered on each stage expressed as a
164 percentage of the emitted recovered dose was considered as the fine particle fraction
165 (FPF). The mass median aerodynamic diameter (MMAD) and FPF were calculated as
166 previously described [19]. Additional experiments were performed in the presence of a
167 neodymium iron boron magnet (e-Magnets UK, Hertfordshire UK) of 20 mm of diameter
168 and 20 mm of length having a maximum energy product (BH_{max}) of 413.8 kJ/m^3 placed
169 on the bottom of the stage 2 of the NGI.

170 **2.2.8 SPIONs concentration assay**

171 SPIONs assay was performed by turbidity measurements at 510 nm. SPIONs were
172 dispersed in 2% w/w poly (vinyl alcohol) (10kDa) solution containing 0.1M of NaOH
173 using a sonicator bath. In the case of formulations containing MgST, particles were
174 dispersed in a 1/1 (v/v) mixture of ethanol and an aqueous solution composed of 2% w/w
175 PVA (10kDa) and 0.1M of NaOH. In these conditions, stable suspensions were obtained.
176 Calibration curves were constructed with standard suspensions composed of SPIONs
177 dispersed in the same media as the formulations and having concentrations ranging from
178 0.001 to 0.05 mg/mL.

179 **2.2.9 Statistical data analysis**

180 Data were statistically evaluated by a two-way ANOVA using Excel[®] software
181 (Microsoft). Significance level was $\alpha < 0.05$.

182

183 **2- Results and discussion**

184 Powder XRD patterns recorded for the powders made of PEG, HP β CD and SPIONs
185 (Fig. 1) had curved baselines and diffraction peaks at 30.3 and 35.6 2θ degrees
186 corresponding to maghemite iron oxide [21]. The intensity of the diffraction peaks
187 increased with an increasing amount of SPIONs incorporated in the formulation. PEG
188 residual crystallinity was also observed in formulations containing more than 33 wt% of
189 PEG from the presence of the two major diffraction peaks at 19.2 and 23.3 2θ degrees
190 [18, 19]. The absence of diffraction peaks corresponding to the HP β CD, suggested that
191 this excipient was in the XRD amorphous state.

192 For spray dried systems comprising PEG, HP β CD and SPIONs, SEM pictures showed
193 individual spherical microparticles surrounded by SPIONs nanoparticles (Figure 2A-B-
194 D). This morphology was obtained due to the high Peclet number of the SPIONs relative
195 to the other excipients, resulting in accumulation on the surface of the microparticles [11,
196 22]. Without PEG in the formulation, heterogeneous blends of free SPIONs and HP β CD
197 microparticles were obtained (data not shown). This failure to form the Trojan
198 microparticles may be as a result of the van der Waals forces between the SPIONs
199 accumulated on the microparticles being too low to enable them be retained on the
200 surface [11] and could also be due to the weak adhesion between HP β CD and SPIONs.
201 Volume weighted particle size distributions of these particles (100H-50F) showed a large
202 proportion of nanoparticles (Fig. 3F). In the absence of HP β CD, large particle aggregates
203 were produced and the presence of SPIONs was not visible (Figure 2C). These
204 aggregates were thought to result from the low and broad melting temperature of the
205 PEG, leading to the formation in the spray dryer of partly solidified sticky particles [18,

206 19]. The absence of visible SPIONs suggests that these soft particles embed SPIONs in
 207 their bulk, before complete solidification. These particles (100P-50F) had the highest
 208 geometric median diameter, as measured by laser diffraction, compared to the other
 209 formulations containing PEG and HP β CD (Fig. 3 - curve A), resulting also in the lowest
 210 specific surface area (Table 2). Due to their large size, these particles were considered to
 211 be not suitable for pulmonary administration. These particles presented the lowest
 212 dispersive surface free energy (γ_s^d) values (36 ± 1 mJ/m²), similar to values found
 213 previously for PEG alone (37.7 ± 4 mJ/m²) [18], confirming that their surfaces were
 214 mainly composed of PEG molecules.

215 **Table 2: Physicochemical properties of the Trojan particles. * Data from supplier.**

	25P-75H-5F	25P-75H-30F	50P-50H-50F	100P-50F	50P-50H-50F-CO3	50P-50H-50F-ST	50P-50H-50F-CO3-ST	SPION
True density (g/cm ³)	1.39 \pm 0.01	1.64 \pm 0.01	1.68 \pm 0.01	1.69 \pm 0.01	1.76 \pm 0.01	1.66 \pm 0.01	1.71 \pm 0.01	2.70 \pm 0.01
Specific surface area (m ² /g)	4.5 \pm 0.2	4.8 \pm 0.2	3.9 \pm 0.1	1.4 \pm 0.2	3.2 \pm 0.1	6.8 \pm 0.4	4.6 \pm 0.3	46.6*
geometric median diameter (μ m)	1.9 \pm 0.2	2.0 \pm 0.4	2.2 \pm 0.4	7.2 \pm 0.7	2.8 \pm 0.3	1.54 \pm 0.2	2.15 \pm 0.3	0.05*
γ_s^d (mJ/m ²)	119 \pm 2	149 \pm 27	43 \pm 5	36 \pm 1	39 \pm 2			
MMAD (μ m)					10.2 \pm 2.0	3.4 \pm 1.1	2.2 \pm 0.8	9.3 \pm 3.1
GSD					2.4 \pm 1.1	2.4 \pm 0.5	2.1 \pm 0.4	4.3 \pm 1.8

216
 217 The use of PEG allowed SPIONs to stick together to form the Trojan microparticles, but
 218 produced large aggregates in the absence of HP β CD. Also, an appropriate ratio between
 219 PEG and HP β CD was necessary to obtain isolated and spherical Trojan microparticles.
 220 Particle deposition on the NGI impactor stages was dependent on the particle type. For
 221 SPIONs alone, only 30% of the nanoparticles emitted out of the gelatin capsule were
 222 deposited beyond the first impactor stage, which has a cut-off aerodynamic diameter of
 223 8.9 μ m (Fig. 5A). According to equation 1, these nanoparticles with a geometric diameter
 224 of 50 nm and having a true density of 4.9 g/cm³ should have an aerodynamic diameter of

225 110 nm and deposit mainly on the filter stage of the impactor. The large deposition on
226 stage 1 is presumably due to the agglomeration of the nanoparticles in non-inhalable
227 large clusters. In fact, SPIONs had a high γ_s^d (147.5 ± 42 mJ/m², Table 1), favouring their
228 aggregation. The increase in PEG concentration in the formulation reduced γ_s^d (Table 2),
229 decreasing the ability of the particles to aggregate. Besides preventing the particles from
230 aggregating, the PEG should also play a role in preventing nonspecific and irreversible
231 adsorption of foreign protein onto the particles, reducing opsonisation and particle
232 phagocytosis.

233 In order to reach the pulmonary alveoli, particles must have an aerodynamic equivalent
234 diameter (d_a) in the 1-5 μ m range [12]. The aerodynamic diameter is the diameter of a
235 sphere of unit density, which reaches the same velocity in the air stream as the particle
236 analysed, which can be nonspherical and have a different density [23, 24]. It is linked to
237 the volume-equivalent geometric diameter (d_g) by the particle shape and density, as
238 described by the following equation [23, 24]:

$$239 \quad d_a = d_g \sqrt{\left(\frac{\rho_p}{\rho_0 \cdot \chi} \right)} \quad \text{Eq. 1}$$

240 Where ρ_0 is the standard particle density (1g/cc), χ is the particle shape factor that is 1 for
241 a sphere and ρ_p is the apparent particle density. ρ_p is equal to the mass of a particle
242 divided by its apparent volume, i.e. the total volume of the particle, excluding open pores,
243 but including closed pores [24], which can be less than the material density (true density)
244 if the particle is porous. Aerodynamic diameter decreases with increasing χ . For an
245 irregular particle χ is always greater than 1 [24]. Also, in order to decrease d_a of large or

246 dense particles below $5\mu\text{m}$, several studies focused on enhancing the particle's porosity
247 to increase χ and decrease ρ_p [11, 15-17].

248 To increase the porosity of the particles, ammonium carbonate $(\text{NH}_4)_2\text{CO}_3$ was added to
249 the formulation. In fact, $(\text{NH}_4)_2\text{CO}_3$ is commonly used as a blowing agent, [12, 25] pore-
250 forming agent [12] or process enhancer [14, 15]. This compound decomposes at 60°C
251 and produces gases during spray drying, thus it is able to create porous or hollow
252 particles. The addition of $(\text{NH}_4)_2\text{CO}_3$ to the PEG-SPIONs mixture did not change the
253 morphology of the particle aggregates (Figure 4A). It would appear that the partially
254 solidified PEG did not allow the formation of void cavities in the particles, which are
255 usually made by material solidification around the gas bubbles produced by the
256 $(\text{NH}_4)_2\text{CO}_3$ decomposition on spray drying. However, the addition of ammonium
257 carbonate to the 50P-50H-50F formulation produced individual spherical and hollow
258 microparticles (Figure 4B). These microparticles had a median geometric diameter of 3
259 μm (Fig. 3) and SPIONs were observable on their surface, but appeared more entrapped
260 than when processing was undertaken in the absence of ammonium carbonate (Figure
261 2D). The deeper penetration of the SPIONs within the microparticles may allow for the
262 avoidance of SPIONs desorption from the surface of the microparticles due to the
263 mechanical stress produced during the dry powder inhalation. The large pores in these
264 microparticles should enhance their aerodynamic properties, and be favourable for
265 alveolar particle deposition.

266 The formulation of SPIONs-loaded microparticles made of PEG and HP β CD with
267 $(\text{NH}_4)_2\text{CO}_3$ (50P-50H-50F- CO_3) decreased the amount of particles collected on stage 1 of
268 the impactor from $49.8\pm 9.0\%$ (for SPIONs alone) to $35.1\pm 6.4\%$, and increased the

269 amount collected on the other stages, with a gradual decrease in the amount deposited
270 with the decrease in the stage cut-off diameter (Fig. 5B). The application of a magnetic
271 field on stage 2 of the impactor changed the particle deposition profile. The percentage of
272 particles on stage 1, 3 and 4 decreased and the percentage on stage 2 significantly
273 increased, 2.5-fold compared to the percentage obtained without magnetic field. Thus,
274 this type of particles was sensitive to the magnetic field; however, their aerodynamic
275 properties were not appropriate for targeting the deep lung area. The aerodynamic
276 properties of the 50P-50H-50F-CO₃ microparticles showed a large measured MMAD
277 value ($10.2 \pm 2.0 \mu\text{m}$) compared to the d_a ($3.66 \mu\text{m}$) calculated with equation 1 using the
278 median volume-weighted geometric diameter D_{50} , considering the particles to be
279 spherical and using the particles' true density (Table 2). This difference can be attributed
280 to the aggregation of the microparticles. Therefore, in order to reduce particle
281 aggregation, magnesium stearate (MgST) was added to the formulation.

282 MgST is used in marketed DPI products (Seebri[®] Breezhaler[®], Novartis; Foradil[®]
283 Certihaler[®], Novartis), and is commonly used to reduce the surface free energy [26] and
284 agglomeration of particles [27]. The carboxylate group of MgST may be coordinated to
285 the iron atom on the SPIONs surface via four different structures, as was previously
286 observed with oleic acid [28]. This would make the SPIONs surface less polar and less
287 adhesive and would change the SPIONs behaviour. However, it was found that the
288 dispersive part of the surface free energy (γ_s^d) of the microparticles was not changed by
289 the addition of MgST. This component of the surface free energy of the Trojan
290 microparticle was already low due to the presence of PEG at the surface. The addition of
291 MgST to the formulations changed the particle morphology. SEM micrographs (Fig. 4C-

292 D) showed individual microparticles with surfaces that appeared more porous compared
293 to particles formulated without MgST (Fig. 4B). This increase in porosity induced an
294 increase in the specific surface area, as measured by nitrogen adsorption (Table 2). Also,
295 rough or irregular particles may have very low effective van der Waals adhesion forces
296 [29], facilitating particle aerosolisation.

297 The addition of MgST into the formulation significantly decreased particle deposition on
298 stage 1 of the NGI, from $49.8 \pm 9.0\%$ for nanoparticles alone to $1.8 \pm 0.3\%$ of the
299 recovered dose for 50P-50H-50F-ST and increased the amount of particles recovered on
300 the other stages (Figure 5C). For the 50P-50H-50F-ST particles the main deposition
301 occurred on stages 2 and 3 (22.9 ± 3.4 and $20.9 \pm 3.4 \%$, respectively), having a cut-off of
302 4.46 and 2.82 μm , respectively, with a gradual decrease in the amount of powder
303 recovered on the other lower cut-off stages. These particles have a MMAD of $3.4 \pm 1 \mu\text{m}$
304 which was higher than the aerodynamic diameter (2.0 μm) calculated using equation 1. In
305 the presence of magnets on stage 2, the amount of particles recovered on this stage
306 increased from 22.9 ± 3.4 to $32.6 \pm 4.9\%$ and decreased on the following stages.

307 The addition of $(\text{NH}_4)_2\text{CO}_3$ and MgST to the formulation improved further the
308 aerodynamic properties of the Trojan particles, leading to the main deposition being
309 centred on stage 4 ($23.4 \pm 3.5\%$) which has a cut-off of 1.6 μm (Figure 5D). In the *in vivo*
310 situation, it would be expected that these particles would be spread out within the whole
311 lung. In the presence of a magnetic field on stage 2, the amount of particles deposited at
312 this stage significantly increased 4-fold from $4.8 \pm 0.7\%$ to $19.5 \pm 3.3\%$. These Trojan
313 particles appeared more sensitive to the magnetic field than particles formulated without

314 $(\text{NH}_4)_2\text{CO}_3$ and MgST and the deposition on the NGI stage was significantly altered in
315 the presence of the magnet (Figure 5D).

316 These particles may be useful for treating localised lung disease, by targeting foci of
317 bacterial infection or tumour nodules. SPIONs released from the Trojan microparticles
318 should be eliminated from the lungs via mechanisms such as mucociliary clearance and
319 macrophage phagocytosis [30]. Even though it has already been used in inhalation in
320 humans, the inhalation of SPIONs may raise some toxicological concerns [31]. A
321 previous toxicological study [32] showed that intratracheally instilled Fe_2O_3
322 nanoparticles of 22 nm diameter could pass through the alveolar-capillary barrier into the
323 systemic circulation at a clearance rate of 3.06 mg/day. The authors of this study
324 suggested that this absorption was probably due to macrophages clearance function
325 overloading, potentially resulting in lung cumulative toxicity of the nanoparticles.

326 PEG used in the formulations discussed here could be useful to prevent early stage
327 particle phagocytosis by alveolar macrophage, by forming a swelling/viscous crown
328 around the drug loaded microparticles to temporarily repulse macrophages [33, 34]. Thus,
329 the use of PEG in the current formulations could decrease the macrophage overloading
330 by slowing down the rate at which the particles are phagocytosed. After complete
331 solubilisation, PEG of 10 kDa should diffuse from the lung into the blood circulation and
332 be eliminated by renal excretion, as its molecular weight is lower than 30kDa [35, 36].

333 Other study performed on rats exposed to magnetite particles with a MMAD of 1.3 μm
334 for 13-week of inhalation showed no mortality, consistent changes in body weights, or
335 systemic toxicity. Elevations of neutrophils in bronchoalveolar lavage appeared to be the
336 most sensitive endpoint of the study [37]. Particle size appears to be determinant in

337 SPIONs toxicity. For example, ultra small superparamagnetic particle of iron oxide
338 having a diameter of 5 nm were not toxic to human monocyte-macrophages *in vitro* and
339 did not activate them to produce pro-inflammatory cytokines or superoxide anions [38].
340 Nevertheless, we suggest that this approach of lung drug targeting by an external
341 magnetic field would be acceptable only in the case of a clear benefit such as in the case
342 of anticancer drug delivery [39] and if used at a low frequency.
343

344 **3- Conclusion**

345 This study demonstrates the feasibility of formulating SPIONs-loaded microparticles
346 which may be useful in the treatment of localised lung disease, such as foci of bacterial
347 infection or tumour nodules. The Trojan microparticles formulated were aerosolised
348 using a dry powder inhaler to produce inhalable particles. These particles were sensitive
349 enough to the magnetic field produced by a commercial magnet to induce a significant
350 change of their distribution on a cascade impactor.

351

352 **4- Acknowledgement**

353 The authors acknowledge funding by a Strategic Research Cluster grant (07/SRC/B1154)
354 under the National Development Plan co-funded by EU Structural Funds and Science
355 Foundation Ireland.

356

- 358 [1] L. Yildirimer, N.T.K. Thanh, M. Loizidou, A.M. Seifalian, Toxicological
359 considerations of clinically applicable nanoparticles, *Nano Today*, 6 (2011) 585-607.
- 360 [2] I. Chourpa, L. Douziech-Eyrolles, L. Ngaboni-Okassa, J.F. Fouquet, S. Cohen-
361 Jonathan, M. Soucé, H. Marchais, P. Dubois, Molecular composition of iron oxide
362 nanoparticles, precursors for magnetic drug targeting, as characterized by confocal
363 Raman microspectroscopy, *Analyst*, 130 (2005) 1395-1403.
- 364 [3] E. Munnier, F. Tewes, S. Cohen-Jonathan, C. Linassier, L. Douziech-Eyrolles, H.
365 Marchais, M. Soucé, K. Hervé, P. Dubois, I. Chourpa, On the interaction of doxorubicin
366 with oleate ions: Fluorescence spectroscopy and liquid-liquid extraction study, *Chemical
367 and Pharmaceutical Bulletin*, 55 (2007) 1006-1010.
- 368 [4] P. Pouponneau, J.C. Leroux, G. Soulez, L. Gaboury, S. Martel, Co-encapsulation of
369 magnetic nanoparticles and doxorubicin into biodegradable microcarriers for deep tissue
370 targeting by vascular MRI navigation, *Biomaterials*, 32 (2011) 3481-3486.
- 371 [5] C. Sapet, L. Le Gourrierc, U. Schillinger, O. Mykhaylyk, S. Augier, C. Plank, O.
372 Zelphati, Magnetofection: Magnetically assisted & targeted nucleic acids delivery, *Drug
373 Delivery Technology*, 10 (2010) 24-29.
- 374 [6] A.L. Coates, Guiding Aerosol Deposition in the Lung, *New England Journal of
375 Medicine*, 358 (2008) 304-305.
- 376 [7] J. Ally, B. Martin, M. Behrad Khamesee, W. Roa, A. Amirfazli, Magnetic targeting of
377 aerosol particles for cancer therapy, *Journal of Magnetism and Magnetic Materials*, 293
378 (2005) 442-449.
- 379 [8] D. Upadhyay, S. Scalia, R. Vogel, N. Wheate, R.O. Salama, P.M. Young, D. Traini,
380 W. Chrzanowski, Magnetised thermo responsive lipid vehicles for targeted and controlled
381 lung drug delivery, *Pharmaceutical Research*, 29 (2012) 2456-2467.
- 382 [9] P. Dames, B. Gleich, A. Flemmer, K. Hajek, N. Seidl, F. Wiekhorst, D. Eberbeck, I.
383 Bittmann, C. Bergemann, T. Weyh, L. Trahms, J. Rosenecker, C. Rudolph, Targeted
384 delivery of magnetic aerosol droplets to the lung, *Nature Nanotechnology*, 2 (2007) 495-
385 499.
- 386 [10] N. Laurent, C. Sapet, L. Le Gourrierc, E. Bertosio, O. Zelphati, Nucleic acid
387 delivery using magnetic nanoparticles: The Magnetofection™ technology, *Therapeutic
388 Delivery*, 2 (2011) 471-482.
- 389 [11] N. Tsapis, D. Bennett, B. Jackson, D.A. Weitz, D.A. Edwards, Trojan particles:
390 Large porous carriers of nanoparticles for drug delivery, *Proceedings of the National
391 Academy of Sciences of the United States of America*, 99 (2002) 12001-12005.

- 392 [12] D.A. Edwards, J. Hanes, G. Caponetti, J. Hrkach, A. Ben-Jebria, M.L. Eskew, J.
393 Mintzes, D. Deaver, N. Lotan, R. Langer, Large porous particles for pulmonary drug
394 delivery, *Science*, 276 (1997) 1868-1871.
- 395 [13] D.E. Geller, J. Weers, S. Heuerding, Development of an inhaled dry-powder
396 formulation of tobramycin using PulmoSphere technology, *J Aerosol Med Pulm Drug*
397 *Deliv*, 24 (2011) 175-182.
- 398 [14] A.M. Healy, B.F. McDonald, L. Tajber, O.I. Corrigan, Characterisation of excipient-
399 free nanoporous microparticles (NPMPs) of bendroflumethiazide, *European Journal of*
400 *Pharmaceutics and Biopharmaceutics*, 69 (2008) 1182-1186.
- 401 [15] L.M. Nolan, L. Tajber, B.F. McDonald, A.S. Barham, O.I. Corrigan, A.M. Healy,
402 Excipient-free nanoporous microparticles of budesonide for pulmonary delivery,
403 *European Journal of Pharmaceutical Sciences*, 37 (2009) 593-602.
- 404 [16] L.M. Nolan, J. Li, L. Tajber, O.I. Corrigan, A.M. Healy, Particle engineering of
405 materials for oral inhalation by dry powder inhalers. II - Sodium cromoglicate,
406 *International Journal of Pharmaceutics*, 405 (2011) 36-46.
- 407 [17] F. Tewes, K.J. Paluch, L. Tajber, K. Gulati, D. Kalantri, C. Ehrhardt, A.M. Healy,
408 Steroid/mucokinetic hybrid nanoporous microparticles for pulmonary drug delivery,
409 *European Journal of Pharmaceutics and Biopharmaceutics*, (2013).
- 410 [18] F. Tewes, O.L. Gobbo, M.I. Amaro, L. Tajber, O.I. Corrigan, C. Ehrhardt, A.M.
411 Healy, Evaluation of HP β CD-PEG microparticles for salmon calcitonin administration
412 via pulmonary delivery, *Molecular Pharmaceutics*, 8 (2011) 1887-1898.
- 413 [19] F. Tewes, L. Tajber, O.I. Corrigan, C. Ehrhardt, A.M. Healy, Development and
414 characterisation of soluble polymeric particles for pulmonary peptide delivery, *European*
415 *Journal of Pharmaceutical Sciences*, 41 (2010) 337-352.
- 416 [20] J. Schultz, L. Lavielle, C. Martin, The role of the interface in carbon-fiber epoxy
417 composites, *J Adhes*, 23 (1987) 45-60.
- 418 [21] G.A. Sotiriou, E. Diaz, M.S. Long, J. Godleski, J. Brain, S.E. Pratsinis, P.
419 Demokritou, A novel platform for pulmonary and cardiovascular toxicological
420 characterization of inhaled engineered nanomaterials, *Nanotoxicology*, 6 (2012) 680-690.
- 421 [22] R. Vehring, Pharmaceutical particle engineering via spray drying, *Pharmaceutical*
422 *Research*, 25 (2008) 999-1022.
- 423 [23] B. Shekunov, P. Chattopadhyay, H.Y. Tong, A.L. Chow, Particle Size Analysis in
424 Pharmaceutics: Principles, Methods and Applications, *Pharmaceutical Research*, 24
425 (2007) 203-227.

- 426 [24] P.F. DeCarlo, J.G. Slowik, D.R. Worsnop, P. Davidovits, J.L. Jimenez, Particle
427 Morphology and Density Characterization by Combined Mobility and Aerodynamic
428 Diameter Measurements. Part 1: Theory, *Aerosol Science and Technology*, 38 (2004)
429 1185-1205.
- 430 [25] D. Traini, P. Young, P. Rogueda, R. Price, In Vitro Investigation of Drug
431 Particulates Interactions and Aerosol Performance of Pressurised Metered Dose Inhalers,
432 *Pharmaceutical Research*, 24 (2007) 125-135.
- 433 [26] V. Swaminathan, J. Cobb, I. Saracovan, Measurement of the surface energy of
434 lubricated pharmaceutical powders by inverse gas chromatography, *International Journal*
435 *of Pharmaceutics*, 312 (2006) 158-165.
- 436 [27] Q.T. Zhou, L. Qu, I. Larson, P.J. Stewart, D.A.V. Morton, Improving aerosolization
437 of drug powders by reducing powder intrinsic cohesion via a mechanical dry coating
438 approach, *International Journal of Pharmaceutics*, 394 (2010) 50-59.
- 439 [28] L.N. Okassa, H. Marchais, L. Douziech-Eyrolles, K. Hervé, S. Cohen-Jonathan, E.
440 Munnier, M. Soucé, C. Linassier, P. Dubois, I. Chourpa, Optimization of iron oxide
441 nanoparticles encapsulation within poly(d,l-lactide-co-glycolide) sub-micron particles,
442 *European Journal of Pharmaceutics and Biopharmaceutics*, 67 (2007) 31-38.
- 443 [29] O.R. Walton, Review of Adhesion Fundamentals for Micron-Scale Particles, *KONA*
444 *Powder and Particle Journal*, 26 (2008) 129-141.
- 445 [30] D.B. Buxton, Nanomedicine for the management of lung and blood diseases,
446 *Nanomedicine*, 4 (2009) 331-339.
- 447 [31] W. Moller, K. Hauszinger, L. Ziegler-Heitbrock, J. Heyder, Mucociliary and long-
448 term particle clearance in airways of patients with immotile cilia, *Respiratory Research*, 7
449 (2006) 10.
- 450 [32] M.T. Zhu, W.Y. Feng, Y. Wang, B. Wang, M. Wang, H. Ouyang, Y.L. Zhao, Z.F.
451 Chai, Particokinetics and extrapulmonary translocation of intratracheally instilled ferric
452 oxide nanoparticles in rats and the potential health risk assessment, *Toxicol Sci.*, 107
453 (2009) 342-351. Epub 2008 Nov 2020.
- 454 [33] I.M. El-Sherbiny, H.D. Smyth, Controlled release pulmonary administration of
455 curcumin using swellable biocompatible microparticles, *Mol Pharm*, 9 (2012) 269-280.
- 456 [34] I.M. El-Sherbiny, S. McGill, H.D. Smyth, Swellable microparticles as carriers for
457 sustained pulmonary drug delivery, *J Pharm Sci*, 99 (2010) 2343-2356.
- 458 [35] C.J. Fee, Size comparison between proteins PEGylated with branched and linear
459 poly(ethylene glycol) molecules, *Biotechnology and Bioengineering*, 98 (2007) 725-731.

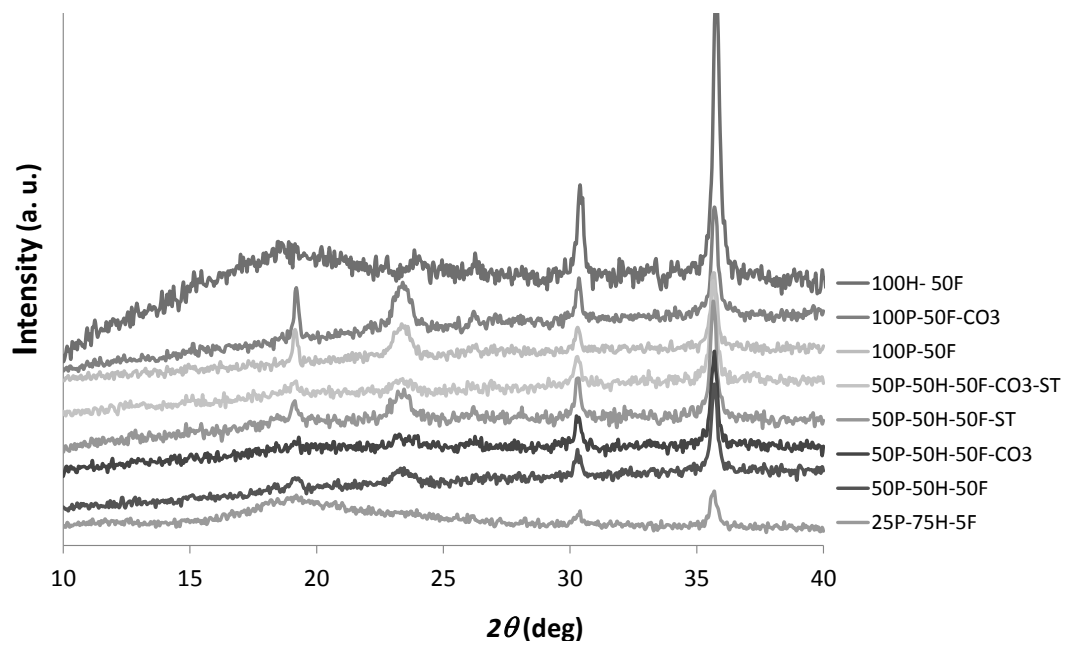
460 [36] J.M. Harris, R.B. Chess, Effect of pegylation on pharmaceuticals, Nat Rev Drug
461 Discov, 2 (2003) 214-221.

462 [37] J. Pauluhn, Subchronic inhalation toxicity of iron oxide (magnetite, Fe₃O₄) in rats:
463 pulmonary toxicity is determined by the particle kinetics typical of poorly soluble
464 particles, Journal of Applied Toxicology, 32 (2012) 488-504.

465 [38] K. Müller, J.N. Skepper, M. Posfai, R. Trivedi, S. Howarth, C. Corot, E. Lancelot,
466 P.W. Thompson, A.P. Brown, J.H. Gillard, Effect of ultrasmall superparamagnetic iron
467 oxide nanoparticles (Ferumoxtran-10) on human monocyte-macrophages in vitro,
468 Biomaterials, 28 (2007) 1629-1642.

469 [39] C. Rudolph, B. Gleich, A.W. Flemmer, Magnetic aerosol targeting of nanoparticles
470 to cancer: nanomagnetosols, Methods in molecular biology (Clifton, N.J.), 624 (2010)
471 267-280.

472



473

474

Figure 1: Powder X-ray diffractograms of hybrid SPION loaded microparticles

475

476

477

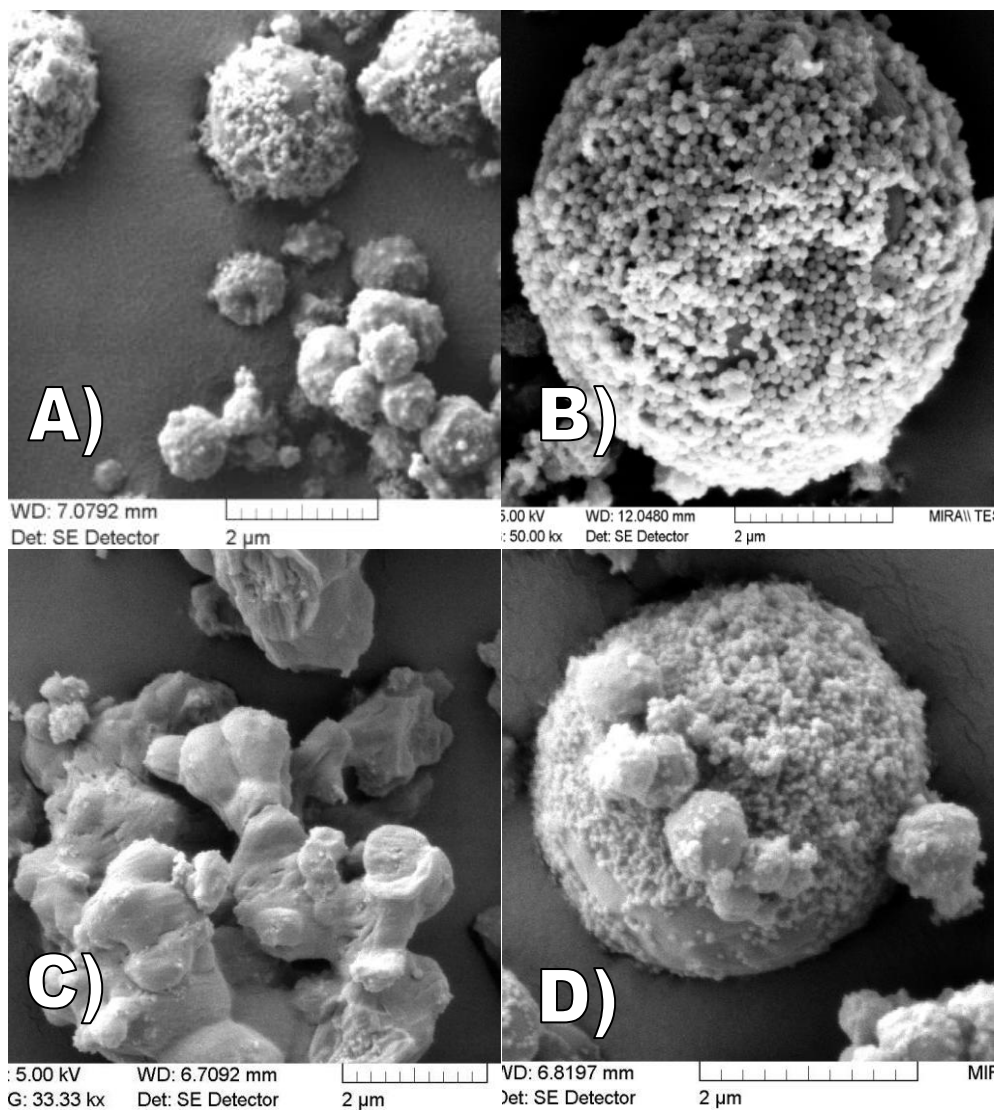
478

479

480

481

482



483

484

485

486

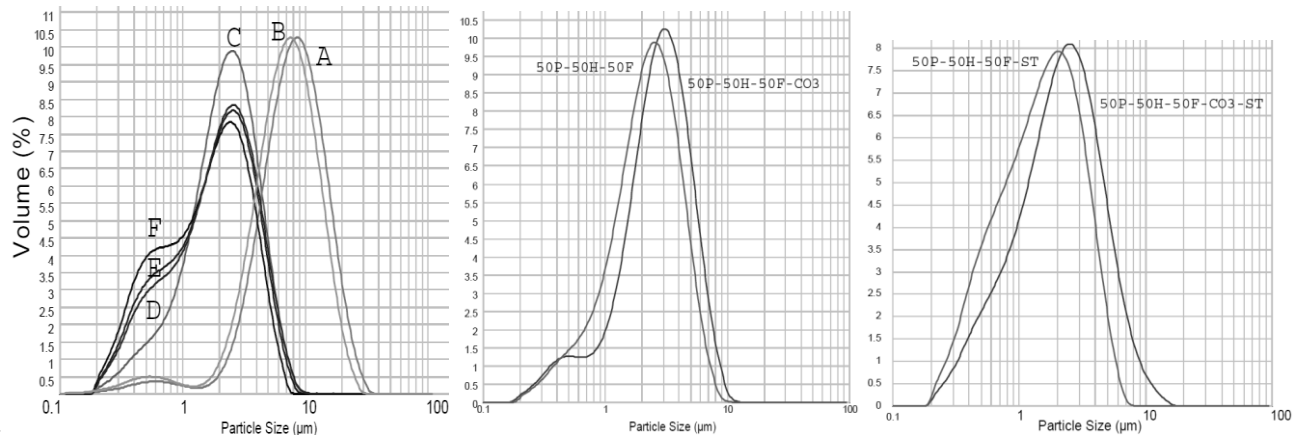
487

488

489 **Figure 2: SEM micrographs of trojan hybrid SPION loaded microparticles: A) 25P-75H-5F B)**

490 **25P-75H-30F C) 100P-50F, D) 50P-50H-50F.**

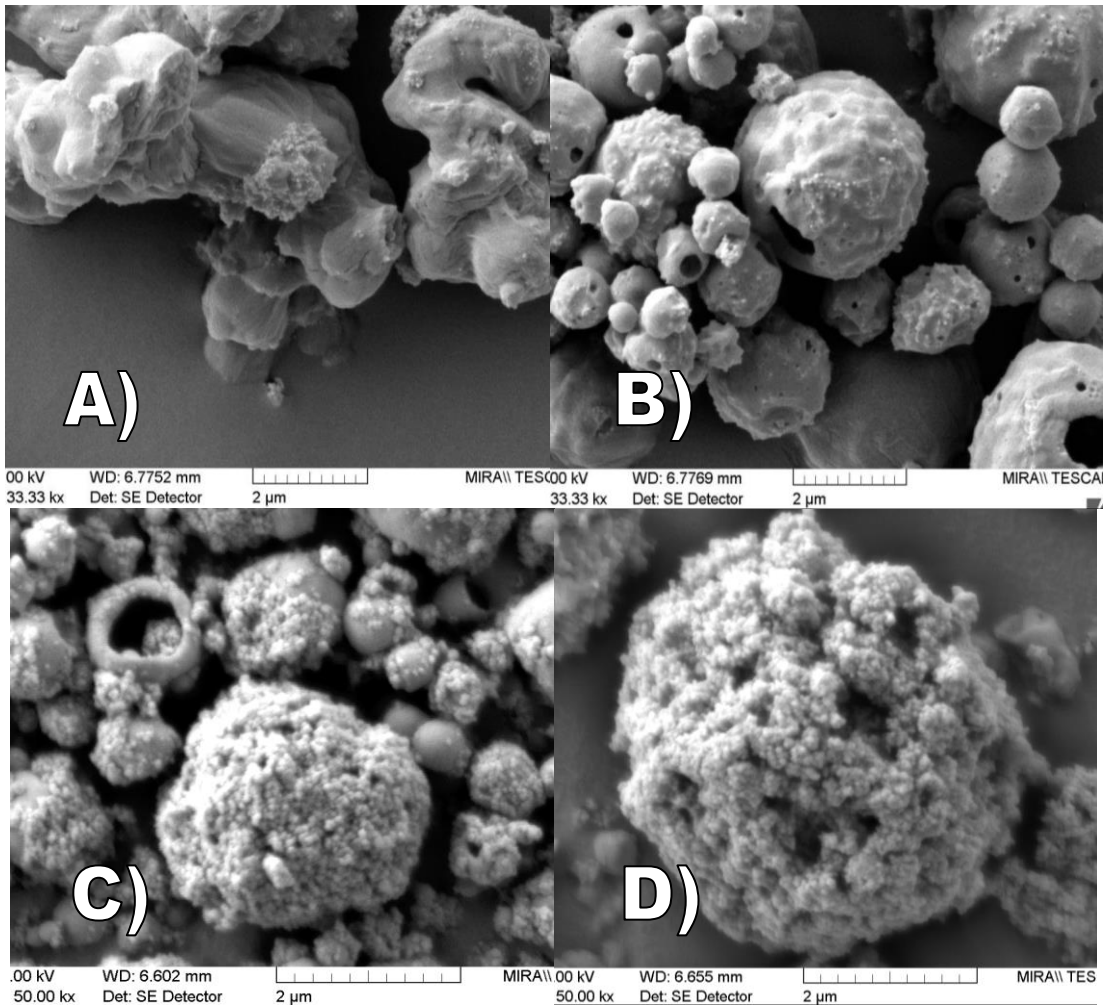
491



492

493 **Figure 3: Geometric particles size distribution of hybrid SPION loaded microparticles. A: 100P-**
 494 **50F; B: 100P-50F-CO3; C: 50P-50H-50F; D: 25P-75H-30F; E: 25P-75H-5F, F: 100HP-50F.**

495



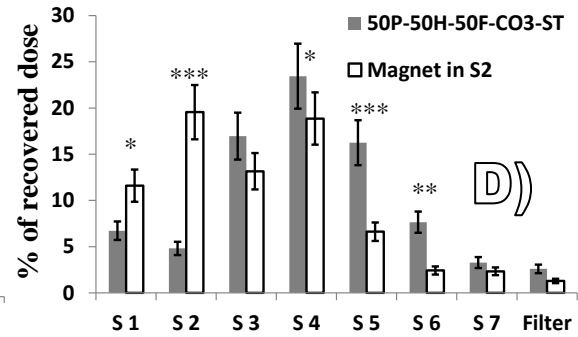
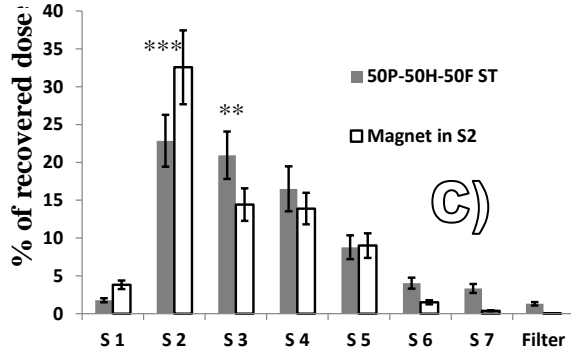
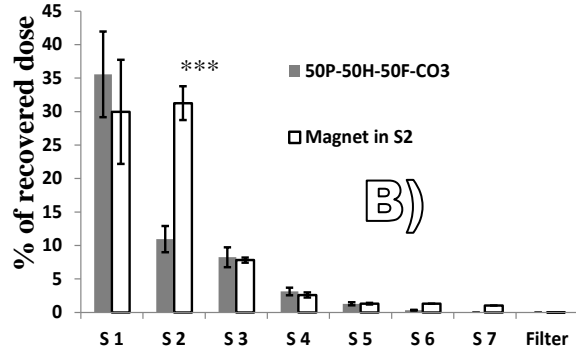
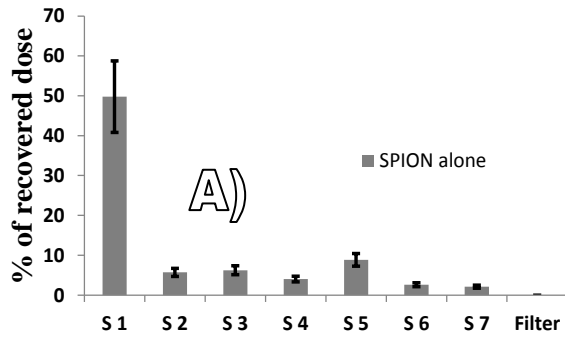
496

497

498 **Figure 4: SEM micrographs of hybrid SPION loaded microparticles formulated with $(\text{NH}_4)_2\text{CO}_3$: A)**
 499 **100P-50F- CO_3 , B) 50P-50H-50F- CO_3 . SEM micrographs of hybrid SPION loaded microparticles**
 500 **formulated with Mg-ST: C) 50P-50H-50F-ST, D) 50P-50H-50F-ST- CO_3 .**

501

502

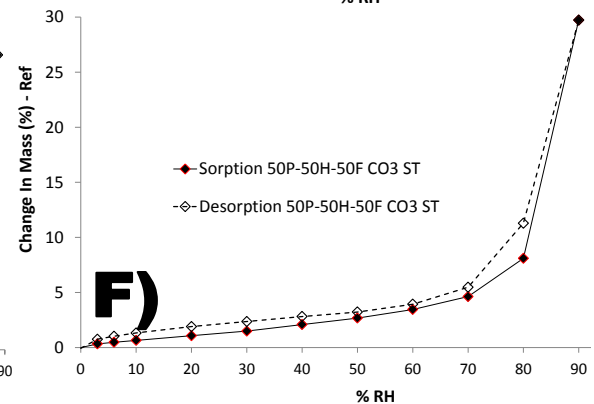
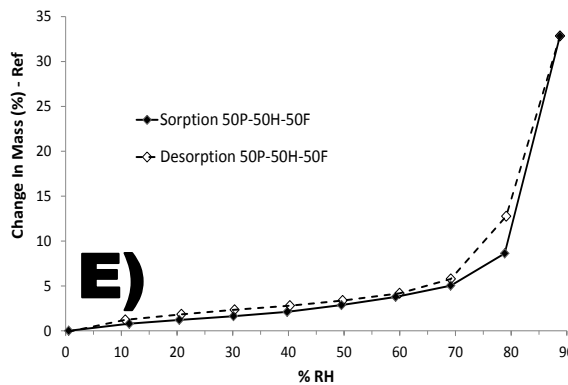
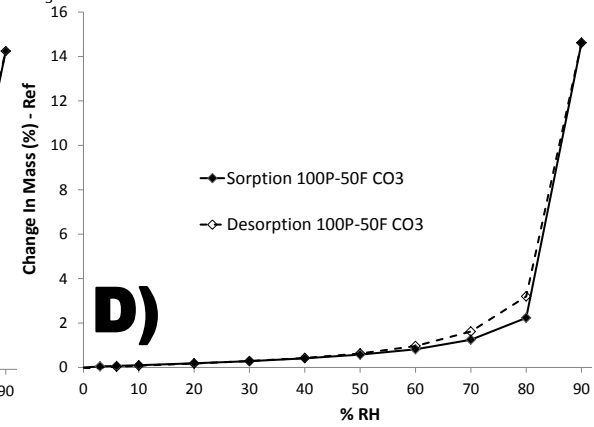
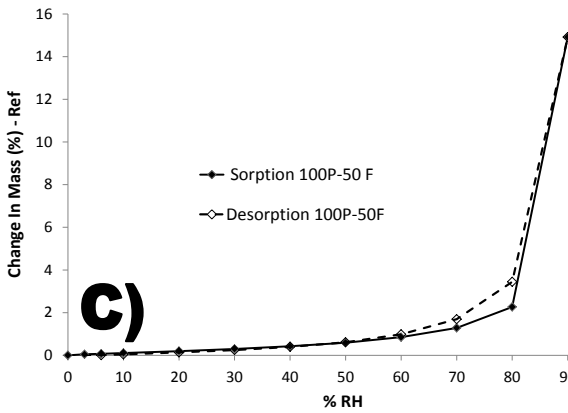
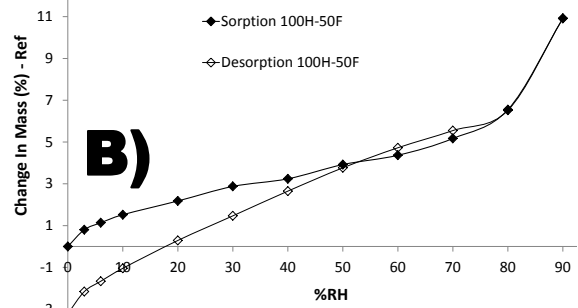
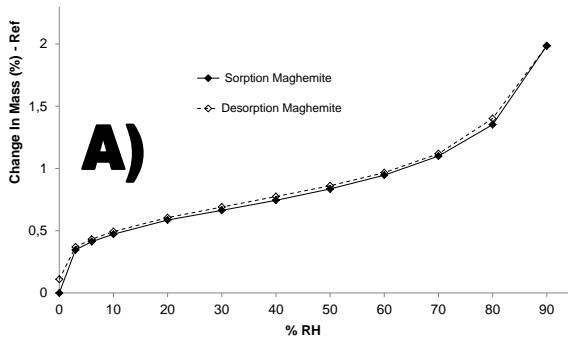


503

504

505 **Figure 5: Mass percentage of the recovered total dose of the trojan microparticles , i.e. the**
 506 **total amount of powder collected from the device, capsule and impactor recovered on each**
 507 **NGI stage, with and without a magnetic field applied on stage 2. Two-way ANOVA, *P < 0.05;**
 508 **** P<0.01; *** P<0.001.**

509



510

511

512

513 Figure 5: Water sorption isotherms. A) SPION alone, B) 100HP-50F, C) 100P-50F, D) 100P-50F-
 514 CO₃, E) 50P-50H-50F, F) 50P-50H-50F-CO₃-ST

515

516